Research in Astron. Astrophys. **2013** Vol. **13** No. **6**, 705–718
http://www.raa-journal.org *http://www.iop.org/journals/raa*

Research in Astronomy and Astrophysics

A magnetic reconnection model for quasi-periodic oscillations in black hole systems *

Chang-Yin Huang[1,2], Ding-Xiong Wang[1], Jiu-Zhou Wang[1] and Zhi-Yun Wang[3]

[1] School of Physics, Huazhong University of Science and Technology, Wuhan 430074, China; *dxwang@mail.hust.edu.cn*
[2] School of Mathematics and Statistics, Huazhong University of Science and Technology, Wuhan 430074, China
[3] School of Physics and Electronic Engineering, Hubei University of Arts and Science, Xiangyang 441053, China

Received 2012 September 17; accepted 2012 December 27

Abstract The quasi-periodic oscillations (QPOs) in black hole (BH) systems with different scales are interpreted based on the magnetic reconnection of large-scale magnetic fields generated by toroidal electric currents flowing in the inner region of the accretion disk, where the current density is assumed to be proportional to the mass density of the accreting plasma. The magnetic connection (MC) is taken into account in resolving dynamic equations describing the accretion disk, in which the MC between the inner and outer disk regions, between the plunging region and the disk, and between the BH horizon and the disk are involved. It turns out that a single QPO frequency associated with several BH systems with different scales can be fitted by invoking the magnetic reconnection due to the MC between the inner and outer regions of the disk, including the BH binaries XTE J1859+226, XTE J1650−500 and GRS 1915+105 and the massive BHs in NGC 5408 X-1 and RE J1034+396. In addition, the X-ray spectra corresponding to the QPOs for these sources are fitted based on the typical disk-corona model.

Key words: accretion, accretion disks — black hole physics — magnetic fields — stars: individual (XTE J1859+226, XTE J1650−500, GRS 1915+105) — galaxies: individual (NGC 5408, RE J1034+396)

1 INTRODUCTION

As is well known, X-ray quasi-periodic oscillation (QPO) is a common phenomenon in radiation from black-hole binaries (BHBs). High-frequency QPOs (HFQPOs) have been observed in several BHBs, some of which show interesting 3:2 frequency pairs (GRS 1915+105, GRO J1655−50, XTE J1550−064, H1743−322), and others display a single QPO (XTE J1859+226, XTE J1650−500). QPOs have also been observed in ultraluminous X-ray sources (ULXs), e.g., a 54 mHz QPO in M82 X-1 and a 20 mHz QPO in NGC 5408 X-1 were discovered respectively by Strohmayer & Mushotsky (2003) and Strohmayer et al. (2007) with XMM-Newton. Strohmayer & Mushotsky

∗ Supported by the National Natural Science Foundation of China.

(2009) discovered another strong 10 mHz QPO in NGC 5408 X-1, and found that the correlation between timing and spectral properties in this source is similar to those of Galactic BHBs.

The first convincing QPO of an active galactic nucleus (AGN) was discovered by Gierlinski et al. (2008) in a narrow line Seyfert 1 RE J1034+396, which opened a window for comparative timing studies of stellar-mass and supermassive black holes (BHs). The ∼1-hour X-ray QPO observed in RE J1034+396 is analogous to the 67 Hz QPO in BHB GRS 1915+105 (Middelton & Done 2010). In earlier years, quasi-periodic signals like QPOs were discovered in some supermassive BHs. For example, the power density spectra of two X-ray flares from Sgr A* observed in 2000 and 2002 show five distinct peaks at periods of ∼100, 219, 700, 1150 and 2250 s (Aschenbach et al. 2004) and a quasi-periodic flux modulation with a period of 22.2 minutes was discovered in the X-ray data of the Sgr A* flare in 2004 (Bélanger et al. 2006).

A number of models have been proposed to interpret HFQPOs in BHBs. However, none of them can fully explain the characteristics of QPOs, especially the correlations of spectral and timing properties (Remillard & McClintock 2006; Maitra & Miller 2010). As is well known, HFQPOs in BHBs are strongly correlated to the steep power law (SPL) state. A successful model of QPOs should include the link to the corresponding spectral state, allowing for a highly dynamic interplay between thermal and nonthermal processes with the mechanisms operating over a wide range of luminosity (Remillard & McClintock 2006). QPOs observed in massive BHs are probably related to the bright state which is similar to the SPL state of BHBs (Strohmayer & Mushotsky 2003, 2009; Middelton et al. 2009), and they may have the same origin as the HFQPOs in BHBs (Gierlinski et al. 2008; Bian & Huang 2010).

Inverse Compton scattering is generally thought to be a promising radiation mechanism associated with the SPL state (Zdziarski 2000; McClintock & Remillard 2006, hereafter MR06), and a disk-corona model is successful in fitting the spectrum of the SPL state (Gan et al. 2009, hereafter G09; Huang et al. 2010). Zhao et al. (2009) (hereafter Z09) interpreted HFQPOs in BHBs as the magnetic reconnection of large-scale magnetic fields generated by toroidal electric currents flowing in the disk without considering the spectral state. In this paper, we improve the Z09 model based on the disk-corona model with magnetic connection (MC) effects. We fit both the QPO frequencies and the corresponding X-ray spectra of five BH systems with different scales, in which three BHBs (XTE J1859+226, XTE J1650–500 and GRS 1915+105), one ULX (NGC 5408 X-1) and one supermassive BH (RE J1034+396) are included.

This paper is organized as follows. A description of the model is given in Section 2. The QPO frequencies and X-ray spectra of the five sources are fitted based on the disk-corona model with MC effects in Section 3. Some issues relating to our model are discussed in Section 4. Throughout this paper, the geometric units $G = c = 1$ are used.

2 MODEL DESCRIPTION

2.1 Origin of Magnetic Fields in BH Systems

Large-scale magnetic fields play very important roles in high energy astrophysical phenomena. The relativistic jets from AGNs and BHBs are launched and collimated by invoking the open large-scale magnetic fields related to the Blandford-Znajek and Blandford-Payne processes (Blandford & Znajek 1977; Blandford & Payne 1982), and the broad iron lines observed in BH systems could be interpreted as the transfer of energy and angular momentum from a spinning BH to its surrounding accretion disk by invoking the magnetic connection via the closed large-scale magnetic fields connecting the horizon with the inner disk (Wilms et al. 2001; Miller et al. 2002; Li 2002a; Wang et al. 2002, hereafter W02). However, a consensus on the origin of large-scale magnetic fields in BH systems has not been reached.

Unlike neutron stars, magnetic fields cannot exist on the horizon of an isolated BH, and they should be maintained by the surrounding environment, such as an accretion disk. For BHBs, mag-

netic fields probably come from the plasma of the companion. One of the most promising origins of large-scale magnetic fields in BH systems is an accretion disk around the BHs, and some authors calculated the magnetic field configurations by assuming there are toroidal electric currents in the disk (Li 2002b; Z09). However, the origin of the currents remains unclear.

In this paper, we intend to interpret the origin of the electric currents based on the assumption that the accreting plasma deviates somewhat from electric neutrality as it flows through the Lagrange point into the Roche lobe of BHBs, resulting in toroidal electric currents flowing in the accretion disk. In addition, we resolve the dynamical equations of the accretion disk by taking the MC effects into account and calculate the mass density and current density in the disk, and then determine the configuration of the large-scale magnetic fields by considering the interaction between the electric current and the disk with an iterative algorithm. It turns out that we can fit the association of QPOs with spectral states in BH systems of different scales based on our model.

The deviation from electric neutrality is described by defining a parameter η as follows,

$$\eta \equiv |n_{\rm e} - n_{\rm p}|/n_{\rm p}\,, \tag{1}$$

where $n_{\rm e}$ and $n_{\rm p}$ are the number densities of electrons and protons, respectively. The charge density can be expressed as

$$\rho_{\rm e} = \eta e n_{\rm p}\,, \tag{2}$$

where $e = 4.8 \times 10^{-10}$ esu is the electron charge.

The large-scale magnetic fields generated by the toroidal electric current may in turn affect the current. For example, the field lines may pipe hot electrons into the corona above the disk and therefore change the charge density in the disk. This effect should be strongest in the inner disk because the magnetic field intensity is strongest near the inner edge of the disk and decreases rapidly outwards. For simplicity, we assume this effect decreases with increasing disk radius as a power law and the surface density of the current in the disk can be expressed as

$$j = \rho_{\rm e} \cdot 2h \cdot \nu_{\rm K} \cdot r^{-n} = \eta e n_{\rm p} \cdot 2h \cdot \Omega_{\rm K} r^{1-n} = \frac{\eta e}{\mu m_{\rm p}} \rho_{\rm m} h \Omega_{\rm K} r^{1-n}\,, \tag{3}$$

where h, $\rho_{\rm m}$ and $m_{\rm p}$ are the half height of the disk, the mass density and the proton mass respectively. The power law index n is a free parameter for fitting the QPO frequency, and $\mu = 0.615$ is the weight-average molecular weight of the gas. The toroidal electric current is assumed to be distributed from the inner edge of the disk to the outer boundary of the disk-corona system, a radius which is set at $r_{\rm out} = 100M$ in calculations, since the radiation of the accretion disk mainly comes from the inner region.

Following the work of Znajek (1978), Linet (1979), Li (2002b) and Z09, we can calculate the toroidal component of the electric vector potential determined by the current given by Equation (3) with a given mass density of disk matter. The boundaries of the inner and outer regions can be determined in terms of the magnetic field configuration. As shown by Figure 1, there are three types of magnetic field configurations generated—the MC of the BH with the disk (MCHD), the MC of the plunging region with the disk (MCPD), and the MC of the inner and outer disk regions (MCDD). In the MCDD region, the magnetic field lines are frozen in the disk at the inner and outer footpoints. The field lines will become twisted since the inner and outer footpoints have different angular velocities.

In Figure 1, the inner and outer footpoints of the field line, shown in red, are located at $r_{\rm in}$ (the inner edge of the disk) and r_0, respectively. The value of the angular velocity difference between the footpoints of this field line is maximal among all the lines in the MCDD region, so this line will first twist itself and trigger the magnetic reconnection, as shown in Figure 2, which periodically releases magnetic energy to generate flares with the frequency being the difference between Keplerian frequencies of the inner and outer footpoints. We interpret this frequency as the QPO frequency, which reads

$$\nu_{\rm QPO} = \frac{\Omega_{\rm K}(r_{\rm in}) - \Omega_{\rm K}(r_0)}{2\pi} = \nu_0 \left[(r_{\rm in}^{3/2} M^{-3/2} + a_*)^{-1} - (r_0^{3/2} M^{-3/2} + a_*)^{-1} \right]\,, \tag{4}$$

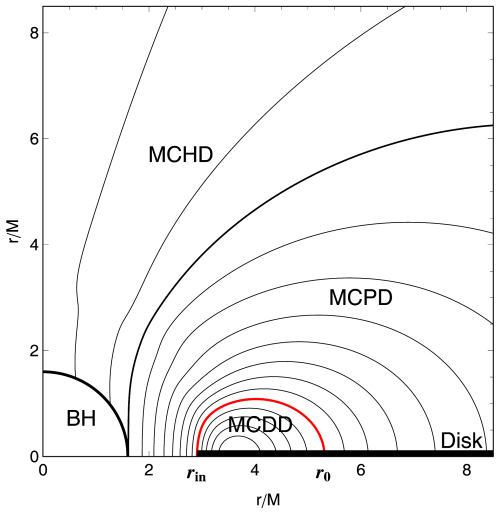

Fig. 1 The configuration of large-scale magnetic fields generated by the continuous distribution of toroidal electric current flowing in the disk. The magnetic field lines are plotted by thin lines and the boundaries between three types of magnetic connection (MCHD, MCPD and MCDD) are shown by thick lines. The red line (*color online*) represents the magnetic field line connecting the radii $r_{\rm in}$ and r_0. The figure is plotted with $m_{\rm BH} = 10$, $a_* = 0.8$, $\dot{m} = 0.1$, $\alpha = 0.3$, $\eta = 10^{-13}$, and $n = 5$, where $\dot{m}$ and α are the mass accretion rate in units of the Eddington accretion rate and the viscosity parameter, respectively.

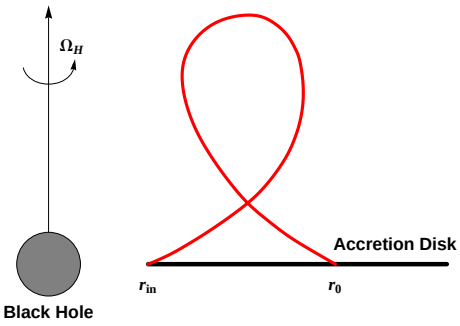

Fig. 2 A schematic drawing of magnetic reconnection in MCDD, where the red line (*color online*) represents the field line connecting radii $r_{\rm in}$ and r_0.

where $\nu_0 \equiv m_{\rm BH}^{-1} 3.23 \times 10^{-4}$Hz and $m_{\rm BH} \equiv M/M_\odot$ is the BH mass in units of the solar mass. $a_* \equiv a/M$ is the dimensionless BH spin. $r_{\rm in}$ is initialized at the innermost stable circular orbit (ISCO).

As shown by Equation (3), parameters n and η determine the current density and therefore the magnetic configuration and QPO frequency once the surface density of disk matter is given. The value of η determines the current intensity and therefore the magnetic field strength, while that of n determines the concentricity of the currents and magnetic fields. A larger n leads to a smaller MCDD region, a smaller distance between $r_{\rm in}$ and r_0, and hence a lower QPO frequency, while a smaller n leads to the opposite results. As an example, a contour of the 190 Hz QPO of XTE J1859+226 is plotted in $\eta - n$ parameter space as shown in Figure 3. It is found that a maximum $\eta \sim 10^{-12}$ is required to avoid too strong of a magnetic field for a stable solution with the MC effect.

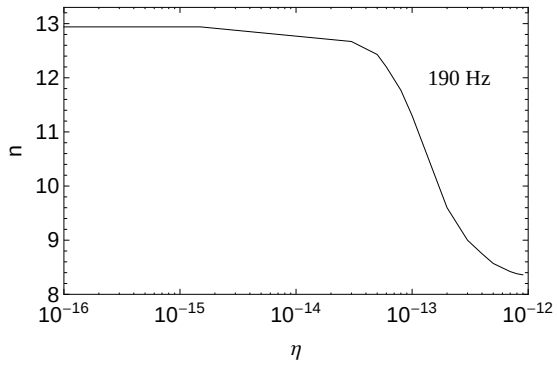

Fig. 3 The contour of a 190 Hz QPO for XTE J1859+226 in $\eta - n$ parameter space with $m_{\rm BH} = 12$, $a_* = 0.96$, $\dot{m} = 0.38$ and $\alpha = 0.3$.

2.2 The Dynamical Equations of Disk and Corona with MC Effects

The dynamical equations of the accretion flow are modified by considering the MC effects on the transfer of energy and angular momentum (Li 2002a; G09),

$$\frac{\mathrm{d}}{\mathrm{d}r}(\dot{M}_{\rm D}L^{\dagger} - g) = 4\pi r(QL^{\dagger} - H_{\rm MC})\,, \tag{5}$$

$$\frac{\mathrm{d}}{\mathrm{d}r}(\dot{M}_{\rm D}E^{\dagger} - g\Omega_i) = 4\pi r(QE^{\dagger} - H_{\rm MC}\Omega_i)\,, \tag{6}$$

where Q and g are respectively the viscously dissipated energy per unit disk surface and interior viscous torque of the disk, and Q consists of two parts,

$$Q = Q_{\rm d} + Q_{\rm cor}\,, \tag{7}$$

where $Q_{\rm d}$ is radiated from the disk as a black body,

$$Q_{\rm d} = \sigma T_{\rm eff}^4\,, \tag{8}$$

and $Q_{\rm cor}$ is transported into the corona to heat it by the magnetic reconnection of tangled small-scale magnetic fields, and it reads (Liu et al. 2002)

$$Q_{\rm cor} = \frac{B_{\rm D}^2}{4\pi}V_{\rm A} = \frac{B_{\rm D}^3}{4\pi\sqrt{4\pi\rho}}\,, \tag{9}$$

where $B_{\rm D}$, $V_{\rm A}$ and ρ are the intensity of the small-scale magnetic fields, the Alfvén speed and mass density, respectively.

The quantity $H_{\rm MC}$ in Equations (5) and (6) is the flux of angular momentum, which reads

$$H_{\rm MC} \equiv \frac{1}{4\pi r}\frac{\mathrm{d}T_{\rm MC}}{\mathrm{d}r} = \frac{1}{2\pi r\mathrm{d}r}\left(\frac{\mathrm{d}\Psi}{2\pi}\right)^2\frac{\Omega_i - \Omega_{i+1}}{\mathrm{d}Z_i}\,, \tag{10}$$

where $\mathrm{d}T_{\rm MC}$ and $\mathrm{d}\Psi$ are the torque exerted on an infinitesimal annulus of the disk and the magnetic flux threading the infinitesimal annulus, respectively.

We can calculate magnetic transfer of energy in a variety of cases of a BH accretion disk by using an equivalent circuit in an analogous way to Macdonald & Thorne (1982) and W02 as shown

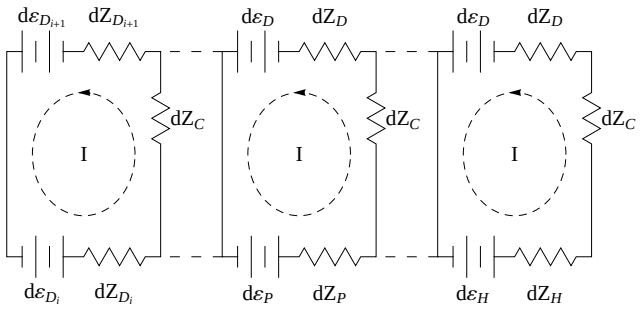

Fig. 4 An equivalent circuit for MCDD, MCPD and MCHD given from left to right, respectively.

in Figure 4. Three types of MC (MCDD, MCPD and MCHD), as indicated in Figure 1, are given in Figure 4, in which a series of loops correspond to the adjacent magnetic surfaces arising from the rotation of the closed field lines.

The quantities $\mathrm{d}Z_{\rm D}$, $\mathrm{d}Z_{\rm P}$, $\mathrm{d}Z_{\rm H}$ and $\mathrm{d}Z_{\rm C}$ are the resistances corresponding to the two adjacent magnetic surfaces in the disk, the plunging region, the BH horizon and the corona, respectively. The quantities $\mathrm{d}\varepsilon_{\rm D}$ and $\mathrm{d}\varepsilon_{\rm H}$ are respectively the electromotive forces generated by the rotation of the disk and the BH horizon as given by W02, and $\mathrm{d}\varepsilon_{\rm P}$ is the electromotive force due to the rotation of the plunging region.

The quantities Ω_i, Ω_{i+1} and $\mathrm{d}Z_i$ in Equations (6) and (10) are explained for the three different disk regions as follows.

(1) **MCDD region:** Ω_i and Ω_{i+1} are respectively the angular velocities of the inner footpoint i and outer footpoint $i+1$ of the closed field line on the disk, and the resistance $\mathrm{d}Z_i$ is defined by

$$\mathrm{d}Z_i = \mathrm{d}Z_{\rm cor} = \frac{R_{\rm cor}\mathrm{d}r}{2\pi r}\,, \tag{11}$$

where $R_{\rm cor}$ is the average areal resistivity of the disk and corona, which is related to $R_{\rm H}$, the surface resistivity of the BH horizon, as follows

$$\begin{cases} R_{\rm cor} = \eta_{\rm R} R_{\rm H} \\ R_{\rm H} = 4\pi = 377\,\Omega. \end{cases} \tag{12}$$

Here $\eta_{\rm R}$ is a parameter to adjust the value of $R_{\rm cor}$. For simplicity, we set $\eta_{\rm R} = 0.1$ in calculations.

(2) **MCHD region:** $\Omega_i = \Omega_{\rm H}$ and $\Omega_{i+1} = \Omega_{\rm D}$ are the angular velocities of the BH horizon and the disk respectively. The resistance

$$\mathrm{d}Z_i = \mathrm{d}Z_{\rm H} + \mathrm{d}Z_{\rm cor}\,, \tag{13}$$

where

$$\mathrm{d}Z_{\rm H} = 2\rho_{\rm H}\mathrm{d}\theta/\varpi\,. \tag{14}$$

The parameters in Equation (14) are given by

$$\varpi = (\Sigma_{\rm H}/\rho_{\rm H})\sin\theta, \qquad \rho_{\rm H}^2 \equiv r_{\rm H}^2 + a^2\cos^2\theta,$$
$$\Sigma_{\rm H} \equiv 2Mr_{\rm H}, \qquad r_{\rm H} = M(1+q), \qquad q = \sqrt{1-a_*^2}\,. \tag{15}$$

(3) **MCPD region:** $\Omega_i = \Omega_{\rm P}$ and $\Omega_{i+1} = \Omega_{\rm D}$ are respectively the angular velocities of the plunging region and the disk, and $\Omega_{\rm P}$ is given as follows (Shapiro & Teukolsky 1983; Wang 2000),

$$\Omega_{\rm P} = \frac{(r-2M)L^\dagger + 2aME^\dagger}{(r^3 + a^2r + 2Ma^2)E^\dagger - 2aML^\dagger}\,. \tag{16}$$

The resistance is the same as that in MCDD expressed by Equation (11).

We adopt the same assumption as given by G09 about the corona: the optical depth of the corona $\tau_{\rm cor} = 1$ and the height of the corona $l = 10r_{\rm ms}$.

3 FITTING THE QPO FREQUENCIES AND X-RAY SPECTRA

In our model, the toroidal electric current interacts with the dynamics of the accretion disk. To solve dynamical Equations (5) and (6), we must know the configuration of the large-scale magnetic fields generated by the toroidal electric current, whose distribution is related to the surface density of matter in the disk by Equation (3), and $\rho_{\rm m}$ is in turn calculated by solving the dynamical equations. For simplicity, we assume that initially there is no electric current in the disk, and solve Equations (5) and (6) with $H_{\rm MC} = 0$ to get the global solution of the disk-corona system. The spectrum from the disk-corona system is then simulated with a Monte Carlo method based on the code developed by G09. The free parameters of the disk-corona model, e.g. BH spin a_* and mass accretion rate $\dot{m}$, can be determined by fitting the observed spectrum. So the surface density of the disk matter is obtained. Then we consider the interaction between the electric current and disk-corona with an iterative algorithm which consists of the following steps:

(i) Assume a value of the power law index n in Equation (3), e.g. $n = 5$.
(ii) Calculate the surface density of the toroidal electric current in the disk and the configuration of the large-scale magnetic fields.
(iii) Resolve the disk-corona system by taking the MC effects into account.
(iv) Repeat steps (ii) and (iii) until the surface density of the disk matter remains stable.
(v) Calculate the frequency $\nu_{\rm QPO}$ by Equation (4).
(vi) Repeat steps (i)-(v) until the QPO frequency agrees with observations.

Steps (ii)–(iii) should be repeated several times before the surface density of disk matter becomes stable. Finally, we simulate the spectrum again and check whether it has changed though it usually has not. Therefore we fitted the spectrum with QPO frequency in agreement with the observation.

As argued by Gan et al. (2007), to avoid the negative radiation flux from the inner disk due to the transfer of energy and angular momentum to the outer disk by the MCDD, we adjust the radius of the inner boundary of the disk to deviate outwards from ISCO. Although the deviation is less than 10% of the radius of the ISCO, it results in a $\sim$30% decrease of QPO frequency.

3.1 Fitting the HFQPOs in XTE J1859+226 and XTE J1650−500 with the SPL State

Observations show that HFQPOs in BHBs are associated with the SPL state which is characterized by a high luminosity (therefore a high accretion rate), strong power-law component and steep power-law index ($\Gamma > 2.4$). We fit the single HFQPOs and the corresponding X-ray spectra of two BHBs: XTE J1859+226 and XTE J1650−500. The comparisons between the simulated spectra and the observed ones for XTE J1859+226 and XTE J1650−500 are shown in Figures 5 and 6, respectively. The total spectra consist of the thermal component emitted from the disk and the power-law component generated by the inverse Compton scattering of soft photons by the relativistic electrons in the corona.

The fitting parameters are listed in Table 1, in which $\dot{m}$ and α are respectively the mass accretion rate in terms of the Eddington accretion rate ($1.4 \times 10^{18} m_{\rm BH}$ g s^{-1}) and the viscosity parameter. The BH mass of XTE J1859+226 was estimated to be in the range 7.6−12$M_\odot$ (MR06). We fit the spectrum of XTE J1859+226 observed on 1999 October 16−18 (MR06) based on the BH mass with upper limit 12 $M_\odot$ and lower limit 7.6 $M_\odot$. Since the BH mass of XTE J1650−500 has not been well estimated, we take a larger mass of 7.3 $M_\odot$ and a smaller one of 4 $M_\odot$, which are estimated by Orosz et al. (2004) to fit the spectrum. A very large BH spin is needed to fit the spectra for the lower limit of the BH mass, and the lower limit of the BH spin corresponding to each BH mass is given in

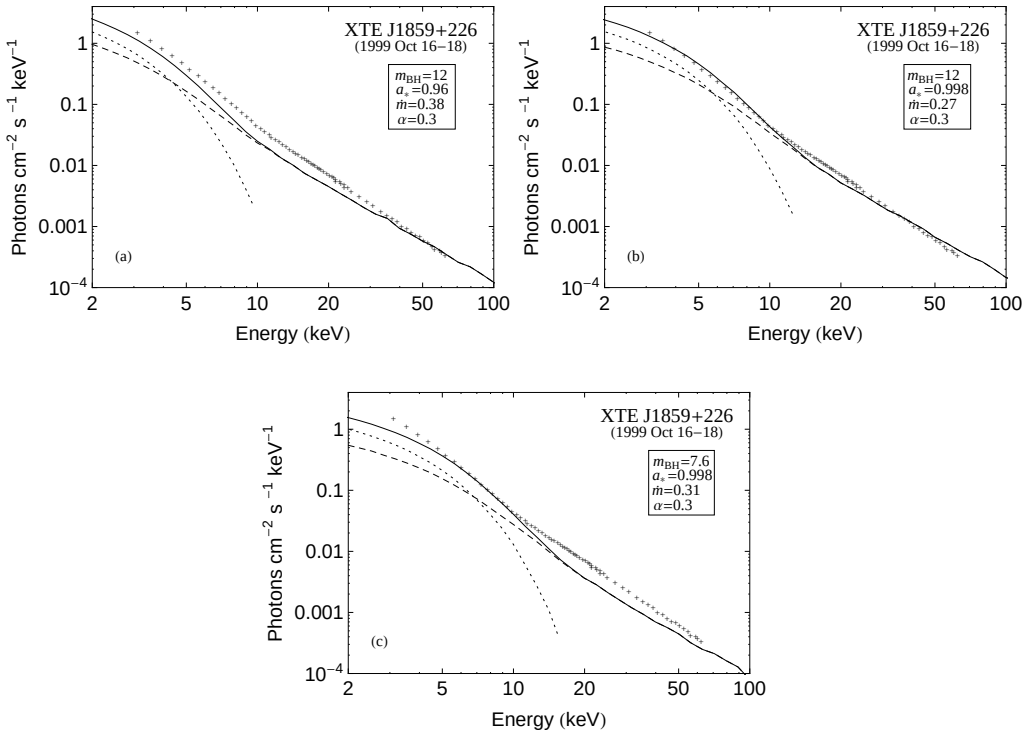

Fig. 5 The simulated spectra of XTE J1859+226 with different parameters: (a) $m_{\rm BH} = 12$, $a_* = 0.96$, $\dot{m} = 0.38$ and $\alpha = 0.3$; (b) $m_{\rm BH} = 12$, $a_* = 0.998$, $\dot{m} = 0.27$ and $\alpha = 0.3$; (c) $m_{\rm BH} = 7.6$, $a_* = 0.998$, $\dot{m} = 0.31$ and $\alpha = 0.3$. The total spectrum and its thermal and Comptonized components are plotted in solid, dotted and dashed lines, respectively. '+' represents the results from observation. The observational data are taken from MR06. The source distance is set at 11 kpc (Zurita et al. 2002; MR06) and an inclination $i = 70^\circ$ is assumed.

Table 1. The spectrum of XTE J1650−500 is fitted with the lower and upper limits of spin for each BH mass, but the spectrum of XTE J1859+226 can only be fitted with an extreme Kerr BH using a lower limit to the BH mass of $7.6M_\odot$. The value of the viscosity parameter α is selected to be in the range 0.1−0.3 to fit the spectrum of each source. The difference in this value probably arises from the difference in the strength of the small-scale magnetic field in the disk if the viscous process is dominated by the tangled small-scale magnetic field. The values of the fitting parameters n and η for QPO frequencies are listed in the last two columns in Table 1. We fix η at a certain value for each scale of BH mass. BH systems with a smaller mass have a stronger magnetic field, that allows a larger value of η. A larger value of n is needed for a smaller BH mass, implying that the toroidal electric currents are concentrated very close to the ISCO.

3.2 QPOs in NGC 5408 X-1 and RE J1034+396

One of the attractive features of our model is that it is applicable in fitting QPOs with corresponding X-ray spectra observed in BH systems with different scales. Strohmayer et al. (2007) discovered a strong 20 mHz QPO in the ULX NGC 5408 X-1, and the X-ray timing and spectral properties are analogous to those exhibited by Galactic stellar-mass BHs in the 'very high' or SPL state. The

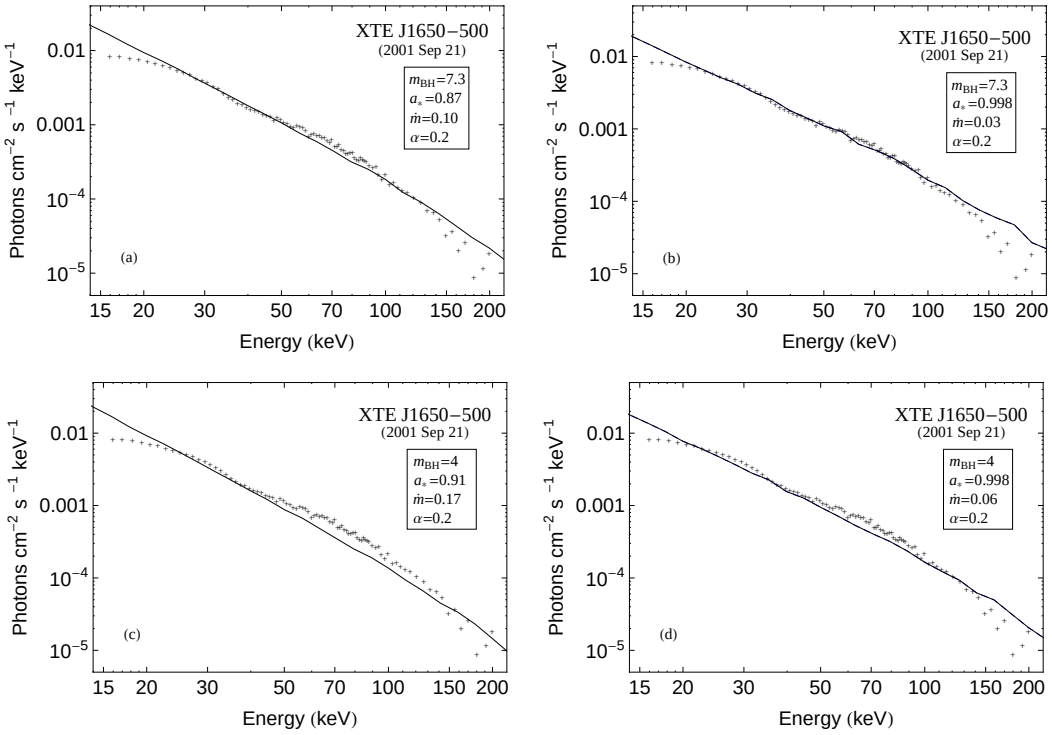

Fig. 6 The simulated spectra of XTE J1650−500 with different parameters: (a) $m_{\rm BH} = 7.3$, $a_* = 0.87$, $\dot{m} = 0.10$ and $\alpha = 0.2$; (b) $m_{\rm BH} = 7.3$, $a_* = 0.998$, $\dot{m} = 0.03$ and $\alpha = 0.2$; (c) $m_{\rm BH} = 4$, $a_* = 0.91$, $\dot{m} = 0.17$ and $\alpha = 0.2$; (d) $m_{\rm BH} = 4$, $a_* = 0.998$, $\dot{m} = 0.06$ and $\alpha = 0.2$. '+' represents the results from observation. The observational data are taken from Miniutti et al. (2004). The source distance is set at 2.6 kpc (Homan et al. 2006) and an inclination of $i = 70^\circ$ is assumed.

fitting parameters for the QPO and X-ray spectrum of NGC 5408 X-1 are also listed in Table 1. The simulated spectra for different parameters and the comparisons to the observed energy spectrum are shown in Figure 7. However, at present, the BH masses in ULXs are permitted to have a wide range from $10^2 M_\odot$ to $10^5 M_\odot$ (Miller et al. 2003; Cropper et al. 2004; Roberts et al. 2005; Wu & Gu 2008). We take a very large BH mass of $10^5 M_\odot$ to fit the data of NGC 5408 X-1 since both the X-ray spectrum and QPO frequency are fitted better for a larger BH mass. The QPO frequency and spectrum are both taken from Strohmayer et al. (2007) with the same hydrogen column density, which are fitted in our model with the lower and upper limits to the BH spin as shown in Table 1.

The first convincing QPO in an AGN was reported by Gierlinski et al. (2008) in RE J1034+396. Middelton & Done (2010) suggest that the QPO discovered in RE J1034+396 is analogous to the 67 Hz QPO seen in the BHB GRS 1915+105, due to their similar 'hot disk dominated' energy spectra. Unlike other HFQPOs, the 67 Hz QPO in GRS 1915+105 is an exceptional case, which appears in the thermal-dominant (TD) state (MR06). In this subsection, we fit both the 67 Hz QPO in GRS 1915+105 and the 0.00027 Hz QPO in RE J1034+396 as a comparison. The spectrum of GRS 1915+105 showing the 67 Hz QPO is taken from Middleton & Done (2010). The spectrum of RE J1034+396 showing the 0.00027 Hz QPO is taken from Middleton et al. (2009) with the same minimum galactic absorption fixed at 1.31×10^{20}cm^{-2}. The 'hot disk dominated' spectra of GRS 1915+105 and RE J1034+396 are both fitted with almost the maximum allowable BH spins

Table 1 The Fitting Parameters for QPO Frequencies and X-ray Spectra

Source	$\nu_{\rm QPO}$(Hz)	$m_{\rm BH}$	a_*	$\dot{m}$	α	n	η
XTE J1859+226	190[a]	12[b]	0.96	0.38	0.3	8.4	
			0.998	0.27	0.3	8.9	
		7.6[b]	0.998	0.31	0.3	14.6	
XTE J1650−500	250[c]	7.3[d]	0.87	0.10	0.2	3.1	
			0.998	0.03	0.2	9.1	10^{-12}
		4[d]	0.91	0.17	0.2	17.7	
			0.998	0.06	0.2	23.1	
GRS 1915+105	67[e]	18[b]	0.998	0.25	0.14	16.9	
		10[b]	0.998	0.40	0.16	27.0	
NGC 5408 X-1	0.02[f]	1.0×10^5	0.95	0.012	0.1	15.1	10^{-16}
			0.998	0.005	0.1	15.5	
RE J1034+396	0.00027[g]	7.0×10^6[h]	0.99	0.15	0.3	16.4	10^{-17}
			0.998	0.14	0.3	16.4	
		2.0×10^6[h]	0.998	0.13	0.3	39.7	10^{-15}

Notes: [a]Cui et al. (2000); [b]MR06; [c]Homan et al. (2003); [d]Orosz et al. (2004); [e]Morgan et al. (1997); [f]Strohmayer et al. (2007); [g]Gierlinski et al. (2008); [h]Zhou et al. (2010).

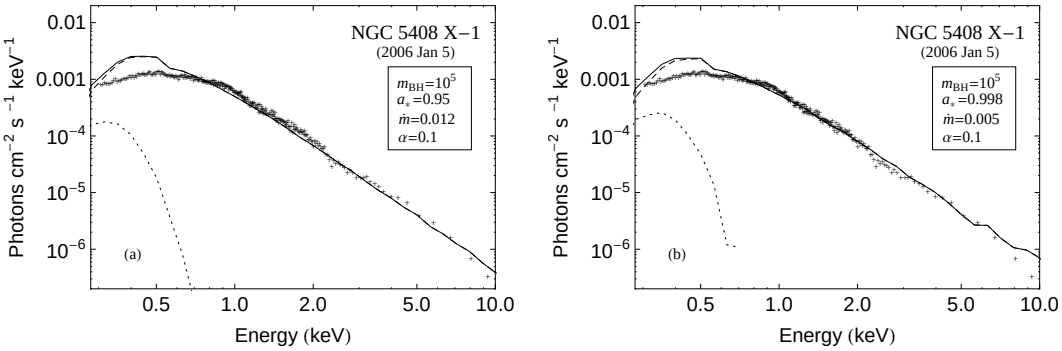

Fig. 7 The simulated spectra of NGC 5408 X-1 with different parameters: (a) $m_{\rm BH} = 10^5$, $a_* = 0.95$, $\dot{m} = 0.012$ and $\alpha = 0.1$; (b) $m_{\rm BH} = 10^5$, $a_* = 0.998$, $\dot{m} = 0.005$ and $\alpha = 0.1$. The plot style is the same as in Figure 5. The observational data are taken from Strohmayer et al. (2007). The source distance is set at 4.8 Mpc (Karachentsev et al. 2002) and an inclination of $i = 75^\circ$ is assumed. The total hydrogen column density is set to be $n_{\rm H} = 13 \times 10^{20}$ cm^{-2} (Strohmayer et al. 2007).

as shown in Table 1, and their comparisons with the observed spectra are shown in Figures 8 and 9, respectively. The disparities between the simulated spectra and the observed ones in the energy bands 10−30 keV for GRS 1915+105 and 0.5−1 keV for RE J1034+396 probably indicate that a second Comptonization process is needed to generate the TD spectrum as shown in figures 10 and 11 of Middelton & Done (2010), where a low temperature, optically thick thermal Comptonization is added to fit the spectra. This Comptonization may be generated from the transition layer between the disk and the corona.

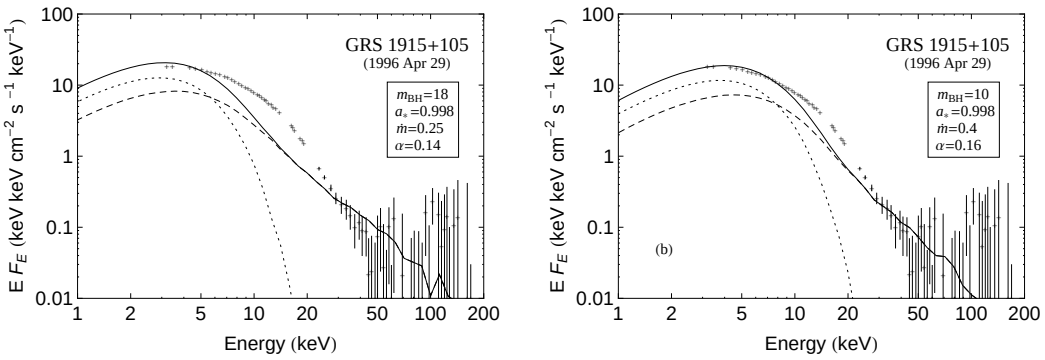

Fig. 8 The simulated spectra of GRS 1915+105 with different parameters: (a) $m_{\rm BH} = 18$, $a_* = 0.998$, $\dot{m} = 0.25$ and $\alpha = 0.14$; (b) $m_{\rm BH} = 10$, $a_* = 0.998$, $\dot{m} = 0.4$ and $\alpha = 0.16$. The plot style is the same as in Fig. 5. The observational data are taken from Middleton & Done (2010). The source distance is set at 11 kpc (McClintock et al. 2006) and an inclination of $i = 66^\circ$ (Fender et al. 1999) is used.

Inspecting Table 1 and Figures 5−9, we find that the QPOs and the corresponding X-ray spectra of BH systems with different scales can be fitted with the magnetic reconnection of the large-scale magnetic fields based on the disk-corona model. QPOs in massive BHs have features similar to those of BHBs, e.g. a very centralized distribution of the electric currents or a large value of n, and its inverse proportionality to BH mass. They are either related to the SPL state, like XTE J1859+226 and XTE J1650−500, or related to the TD state, like GRS 1915+105. These similar characteristics probably hint that QPOs in BH systems with different scales may have the same origin and are associated with the same spectral state.

4 DISCUSSION

In this paper, a toy model for the QPOs in BH systems with different scales is proposed based on the magnetic reconnection of large-scale magnetic fields generated by toroidal electric currents in the disk. The dynamical equations of the accretion disk are resolved based on the interaction between electric currents with the disk-corona system using an iterative algorithm. The 190 Hz and 250 Hz single HFQPOs in BHBs XTE J1859+226 and XTE J1650−500 associated with the SPL states are well fitted based on the disk-corona model with electric currents flowing in the inner disk. Similar QPOs observed in ULX NGC 5408 X-1 and Seyfert 1 AGN RE J1034+396, and the corresponding X-ray spectra, are also fitted. The spectrum of NGC 5408 X-1 is fitted with a strong power-law component and a steep power-law index, suggesting that its QPO is similar to the HFQPOs in BHBs XTE J1859+226 and XTE J1650−500, all of which are probably associated with the same spectral state — SPL state. The QPO in RE J1034+396 is analogous to the 67 Hz QPO in GRS 1915+105, which is associated with the TD state.

Similarities between QPOs in BH systems with different scales enable us to estimate some of the physical quantities of massive BHs which have not been well constrained at present. As suggested by MR06, the frequencies of HFQPOs in BHBs showing 3:2 frequency pairs are inversely proportional to the BH mass. Abramowicz et al. (2007) used the $1/M$ scaling to calculate expected QPO frequencies for BHs with different scales and neutron stars. Similarly, we can use this relationship to estimate the BH mass in ULX NGC 5408 X-1. Including the three BHBs showing a single HFQPO, we have the relationship, $m_{\rm BH} = 1460\nu_{\rm QPO}^{-1}$, between the BH mass and the QPO frequency as shown

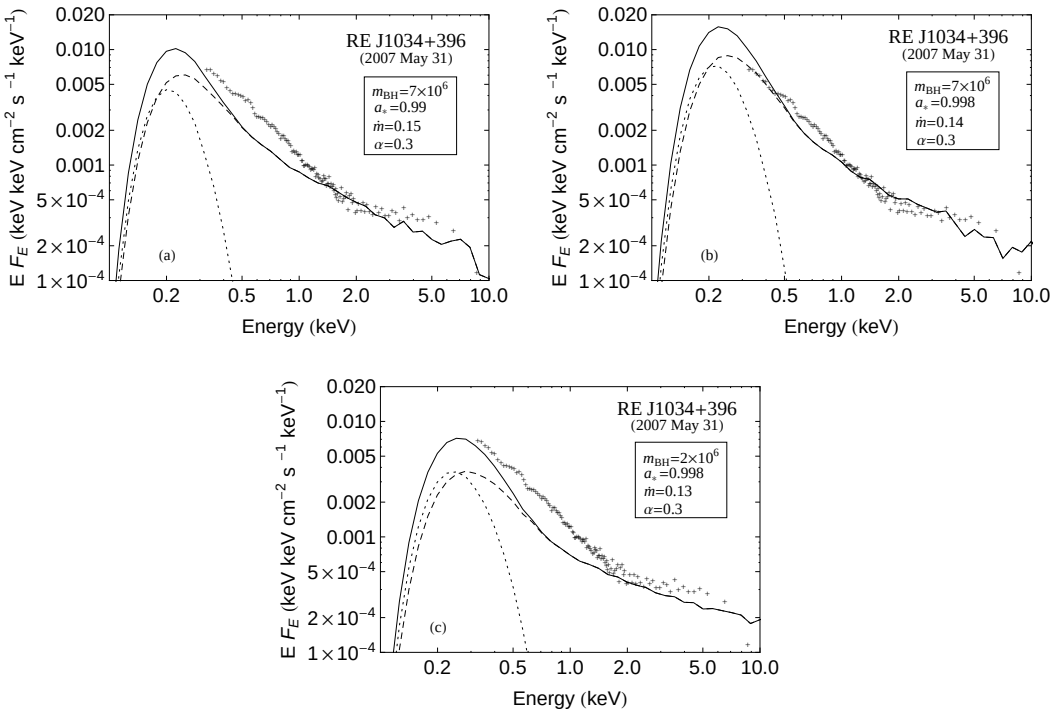

Fig. 9 The simulated spectra of RE J1034+396 with different parameters: (a) $m_{\rm BH} = 7 \times 10^6$, $a_* = 0.99$, $\dot{m} = 0.15$ and $\alpha = 0.3$; (b) $m_{\rm BH} = 7 \times 10^6$, $a_* = 0.998$, $\dot{m} = 0.14$ and $\alpha = 0.3$; (c) $m_{\rm BH} = 2 \times 10^6$, $a_* = 0.998$, $\dot{m} = 0.13$ and $\alpha = 0.3$. The plot style is the same as in Fig. 5. The observational data are taken from Middleton et al. (2009). The source distance is set at 125.9 Mpc (z=0.042, H_0=100 km s^{-1} Mpc^{-1}) and an inclination $i = 40^\circ$ is assumed. We only consider the minimum galactic absorption fixed at 1.31×10^{20} cm^{-2} (Middleton et al. 2009).

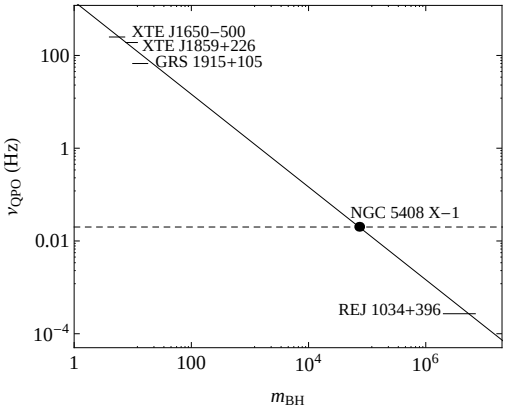

Fig. 10 Relationship between BH mass and QPO frequency. The relationship is fitted with $m_{\rm BH} = 1460\nu_{\rm QPO}^{-1}$ shown by the skewed line. The short horizontal lines represent the ranges of BH mass for the sources. NGC 5408 X-1 is shown on the skewed line (*black dot*) corresponding to the 0.02 Hz QPO (*dashed line*).

in Figure 10. The BH mass of NGC 5408 X-1 is then estimated to be about $7.3 \times 10^4 M_\odot$ with a 0.02 Hz QPO as shown by the black dot in Figure 10.

The quasi-periodic signals similar to QPOs were also discovered in the X-ray flux of Sgr A*. If these signals are indeed QPOs and are triggered by the magnetic reconnection described in this paper, then the lower limit of the BH spin can be constrained because the outer footpoints of the magnetic field lines cannot extend to an infinite distance. We estimate the lower limit of the BH spin of Sgr A* to be 0.448 by fitting the 22.2 minutes of signal discovered in the X-ray flare on 2004 August 31 (Bélanger et al. 2006) using the mass $4.4 \times 10^6 M_\odot$ (Genzel et al. 2010), which is very close to the value of $a_* \approx 0.44 \pm 0.08$ estimated by Kato et al. (2010) using the QPO method in the context of disk-seismology.

We have noticed that the upper and lower kHz QPOs of accreting X-ray binaries are interpreted as Alfvén wave oscillations with different densities in the accreted material at a preferred radius near the star's surface, and this model successfully explains the empirical relationship between the upper and lower kHz QPO frequencies and the linear relationship between the high and low QPO frequencies of BHs, neutron stars and white dwarfs (Zhang 2004; Zhang et al. 2007). The idea of interpreting QPOs with magnetic reconnection proposed in this paper may also apply to neutron stars and other astrophysical objects. For example, QPOs can be interpreted as the reconnection of the magnetic field on the surface of a neutron star, then the model evolves to the beat frequency model (e.g., Miller et al. 1998), providing a physical mechanism for producing QPOs.

Magnetic reconnection is being increasingly recognized as an important process in high energy objects, such as stellar X-ray flares, accretion disk coronas, and magnetar flares. In this paper, we apply it to interpret the QPOs in BH systems with different scales based on a possible origin of the large-scale magnetic field in the BH accretion disk. The magnetic fields generated in the inner disk by the electric currents are $\sim 10^6$ and $\sim 10^3$ Gauss for BHBs and AGNs respectively. Although the strength of these fields is much less than that of the tangled small-scale magnetic fields in the disk, the magnetic reconnection of large-scale magnetic fields should have some effect on the heating of the corona, and these should be considered in future work. Furthermore, the influence of the magnetic reconnection on X-ray spectra is another open question.

Acknowledgements We are very grateful to the anonymous referee for his/her helpful comments on the manuscript. This work is supported by the National Natural Science Foundation of China (Grant Nos. 11173011, 11143001, 11103003 and 11045004), the National Basic Research Program of China (973 program, 2009CB824800) and the Fundamental Research Funds for the Central Universities (HUST: 2011TS159).

References

Abramowicz, M. A., Kluzniak, W., Bursa, M., et al. 2007, RevMexAA (Serie de Conferencias), 27, 8

Aschenbach, B., Grosso, N., Porquet, D., & Predehl, P. 2004, A&A, 417, 71

Bélanger, G., Terrier, R., de Jager, O. C., Goldwurm, A., & Melia, F. 2006, Journal of Physics Conference Series, Proceedings of "The Universe Under the Microscope - Astrophysics at High Angular Resolution", eds. Rainer Schoedel, Andreas Eckart, Susanne Pfalzner and Eduardo Ros, 54, 420

Bian, W.-H., & Huang, K. 2010, MNRAS, 401, 507

Blandford, R. D., & Znajek, R. L. 1977, MNRAS, 179, 433

Blandford, R. D., & Payne, D. G. 1982, MNRAS, 199, 883

Cropper, M., Soria, R., Mushotzky, R. F., et al. 2004, MNRAS, 349, 39

Cui, W., Shrader, C. R., Haswell, C. A., & Hynes, R. I. 2000, ApJ, 535, L123

Fender, R. P., Garrington, S. T., McKay, D. J., et al. 1999, MNRAS, 304, 865

Gan, Z.-M., Wang, D.-X., & Lei, W.-H. 2009, MNRAS, 394, 2310 (G09)

Gan, Z.-M., Wang, D.-X., & Li, Y. 2007, MNRAS, 376, 1695

Genzel, R., Eisenhauer, F., & Gillessen, S. 2010, Reviews of Modern Physics, 82, 3121
Gierliński, M., Middleton, M., Ward, M., & Done, C. 2008, Nature, 455, 369
Homan, J., Klein-Wolt, M., Rossi, S., et al. 2003, ApJ, 586, 1262
Homan, J., Wijnands, R., Kong, A., et al. 2006, MNRAS, 366, 235
Huang, C.-Y., Gan, Z.-M., Wang, J.-Z., & Wang, D.-X. 2010, MNRAS, 403, 1978
Karachentsev, I. D., Sharina, M. E., Dolphin, A. E., et al. 2002, A&A, 385, 21
Kato, Y., Miyoshi, M., Takahashi, R., Negoro, H., & Matsumoto, R. 2010, MNRAS, 403, L74
Li, L.-X. 2002a, ApJ, 567, 463
Li, L.-X. 2002b, Phys. Rev. D, 65, 084047
Linet, B. 1979, Journal of Physics A Mathematical General, 12, 839
Liu, B. F., Mineshige, S., & Shibata, K. 2002, ApJ, 572, L173
MacDonald, D., & Thorne, K. S. 1982, MNRAS, 198, 345
Maitra, D., & Miller, J. M. 2010, ApJ, 718, 551
McClintock, J. E., & Remillard, R. A. 2006, Black Hole Binaries, in Compact Stellar X-ray Sources, eds. W. H. G., Lewin and M., van der Klis (Cambridge: Cambridge Univ. Press), 157 (MR06)
McClintock, J. E., Shafee, R., Narayan, R., et al. 2006, ApJ, 652, 518
Middleton, M., Done, C., Ward, M., Gierliński, M., & Schurch, N. 2009, MNRAS, 394, 250
Middleton, M., & Done, C. 2010, MNRAS, 403, 9
Miller, M. C., Lamb, F. K., & Psaltis, D. 1998, ApJ, 508, 791
Miller, J. M., Fabian, A. C., Wijnands, R., et al. 2002, ApJ, 570, L69
Miller, J. M., Fabbiano, G., Miller, M. C., & Fabian, A. C. 2003, ApJ, 585, L37
Miniutti, G., Fabian, A. C., & Miller, J. M. 2004, MNRAS, 351, 466
Morgan, E. H., Remillard, R. A., & Greiner, J. 1997, ApJ, 482, 993
Orosz, J. A., McClintock, J. E., Remillard, R. A., & Corbel, S. 2004, ApJ, 616, 376
Remillard, R. A., & McClintock, J. E. 2006, ARA&A, 44, 49
Roberts, T. P., Warwick, R. S., Ward, M. J., Goad, M. R., & Jenkins, L. P. 2005, MNRAS, 357, 1363
Shapiro, S. L., & Teukolsky, S. A. 1983, Black Holes, White Dwarfs, and Neutron Stars: The Physics of Compact Objects (New York: John Wiley and Sons)
Strohmayer, T. E., & Mushotzky, R. F. 2003, ApJ, 586, L61
Strohmayer, T. E., & Mushotzky, R. F. 2009, ApJ, 703, 1386
Strohmayer, T. E., Mushotzky, R. F., Winter, L., et al. 2007, ApJ, 660, 580
Wang D.-X., 2000, General Relativity and Gravitation, 32, 553
Wang, D. X., Xiao, K., & Lei, W. H. 2002, MNRAS, 335, 655 (W02)
Wilms, J., Reynolds, C. S., Begelman, M. C., et al. 2001, MNRAS, 328, L27
Wu, Q., & Gu, M. 2008, ApJ, 682, 212
Zdziarski, A. A. 2000, in Highly Energetic Physical Processes and Mechanisms for Emission from Astrophysical Plasmas, IAU Symposium, 195, eds. P. C. H. Martens, S. Tsuruta, & M. A. Weber, 153
Zhang, C. 2004, A&A, 423, 401
Zhang, C. M., Yin, H. X., & Zhao, Y. H. 2007, PASP, 119, 393
Zhao, C.-X., Wang, D.-X., & Gan, Z.-M. 2009, MNRAS, 398, 1886 (Z09)
Zhou, X.-L., Zhang, S.-N., Wang, D.-X., & Zhu, L. 2010, ApJ, 710, 16
Znajek, R. L. 1978, MNRAS, 182, 639
Zurita, C., Sánchez-Fernández, C., Casares, J., et al. 2002, MNRAS, 334, 999